Since January 2020 Elsevier has created a COVID-19 resource centre with free information in English and Mandarin on the novel coronavirus COVID-19. The COVID-19 resource centre is hosted on Elsevier Connect, the company's public news and information website.

Carbohydrate Polymers 299 (2023) 120173

Contents lists available at ScienceDirect

Carbohydrate Polymers

journal homepage: www.elsevier.com/locate/carbpol

Inhibitory activity of a sulfated oligo-porphyran from *Pyropia yezoensis* against SARS-CoV-2

Lihua Geng [a,b], Quanbin Zhang [a,b], Qishan Suo [a,b,c], Jing Wang [a,b], Yingxia Wang [d], Cong Wang [e], Ning Wu [a,b,f,*]

[a] CAS and Shandong Province Key Laboratory of Experimental Marine Biology, Center for Ocean Mega-Science, Institute of Oceanology, Chinese Academy of Sciences, Qingdao, China
[b] Laboratory for Marine Biology and Biotechnology, Qingdao National Laboratory for Marine Science and Technology, Qingdao, China
[c] University of Chinese Academy of Sciences, Beijing, China
[d] Public Technology Service Center, Center for Ocean Mega-Science, Institute of Oceanology, Chinese Academy of Sciences, Qingdao, China
[e] School of Medicine and Pharmacy, Ocean University of China, Qingdao, China
[f] Nantong Zhongke Marine Science and Technology Research and Development Center, Nantong, China

ARTICLE INFO

Keywords:
Pyropia yezoensis
Oligo-porphyran
Oligosaccharide
SARS-CoV-2
SPR
Pseudovirus test

ABSTRACT

COVID-19 caused by SARS-CoV-2 has spread around the world at an unprecedented rate. A more homogeneous oligo-porphyran with mean molecular weight of 2.1 kD, named OP145, was separated from *Pyropia yezoensis*. NMR analysis showed OP145 was mainly composed of →3)-β-D-Gal-(1 → 4)-α-L-Gal (6S) repeating units with few replacement of 3,6-anhydride, and the molar ratio was 1:0.85:0.11. MALDI-TOF MS revealed OP145 contained mainly tetrasulfate-oligogalactan with Dp range from 4 to 10 and with no more than two 3,6-anhydro-α-L-Gal replacement. The inhibitory activity of OP145 against SARS-CoV-2 was investigated *in vitro* and *in silico*. OP145 could bind to Spike glycoprotein (S-protein) through SPR result, and pseudovirus tests confirmed that OP145 could inhibite the infection with an EC50 of 37.52 μg/mL. Molecular docking simulated the interaction between the main component of OP145 and S-protein. All the results indicated that OP145 had the potency to treat and prevent COVID-19.

1. Introduction

COVID-19 is caused by severe acute respiratory syndrome associated coronavirus-2 (SARS-CoV-2). By now, it has infected over 600 million people and >6 million were dead because of infection. The ongoing COVID-19 pandemic has become a major threat to public health and social stability (World Health Organization, 2020). Effective therapies to treat or prevent COVID-19 are urgently needed. Marine-derived sulfated polysaccharides (MSP), particularly the sulfated polysaccharides from red algae, which made up >40 % of that antiviral MSP, have already been reported for their potent inhibitory effects on virus infection (Singh, Chauhan, & Kuddus, 2021). Different kinds of carrageenans and sulfated galactans extracted from red algae exhibited selective antiviral activity against herpes simplex virus (HSV) types 1 and 2 (Mazumder et al., 2002), and human immunodeficiency virus (HIV) types 1 and 2 (Bouhlal et al., 2011; Witvrouw et al., 1994). Besides the shielding effect on viral attachment and entry of sulfated polysaccharides, several sulfated polysaccharides have been found able to hinder the fusion events that occur between viral and host cell membranes, which can bind to fusion proteins and inactivate them by declining their hydrophobic properties. For example, a sulfated glucuronorhamnan obtained from *Monostroma nitidum* was reported to bind with virus particles to inhibit the EV71 virus adsorption and retard the virus lifecycle by down-regulating host phosphoinositide 3-kinase/protein kinase B signaling pathway in Madin-Darby canine kidney cells (Wang et al., 2020). Considering to the multiply effects of MSP on anti-virus, researchers reported recently that MSP possessed inhibitory properties against SAR-CoV-2 (Salih et al., 2021). Song et al. (2020) reported that 4 MSP showed the activities against SARS-CoV-2 including sea cucumber sulfated polysaccharide, fucoidan from brown algae, iota-carrageenan from red algae and chondroitin sulfate C from sharks. Kwon et al. (2020) also reported that fucoidan extracted from the seaweed *Saccharina japonica* was able to compete with heparin for S-protein binding. Beside, ι-carrageenan from red algae could inhibit SARS-CoV-2 in cell

* Corresponding author at: Nantong Zhongke Marine Science and Technology Research and Development Center, Nantong, China.
E-mail address: wuning@qdio.ac.cn (N. Wu).

https://doi.org/10.1016/j.carbpol.2022.120173
Received 5 December 2021; Received in revised form 24 September 2022; Accepted 26 September 2022
Available online 30 September 2022

culture and inhibit the cell entry of the SARS-CoV-2 spike pseudotyped lentivirus in a dose dependent manner (Bansal et al., 2020; Morokutti-Kurz et al., 2021), which showed the huge potent of MSP to treat and prevent the ongoing COVID-19.

Pyropia yezoensis, kind of red algae, is one of the most important economic algae in China, and is very common in people's diets and foods. *P. yezoensis* contains up to 20 % porphyran, as well as other biofunctional compounds, such as proteins, vitamins, minerals, eicosapentaenoic acid, carotenoids (**Geng, Wang, Zhang, Yue, & Zhang,** 2019). Porphyran and oligo-porphyran exhibit a series of biological activities, including antioxidant, immunomodulatory and anti-tumour activity (**Qiu, Jiang, Fu, Ci, & Mao,** 2021), while oligo-porphyran exhibits some unique biological activities such as neuroprotective activity (Liu et al., 2018), nephroprotective activity (**Wang, Hou, Duan, & Zhang,** 2017) and alleviating nonalcoholic fatty liver disease (Wang et al., 2021). Besides, oligo-porphyran exhibited stronger antioxidant activity compared with native porphyan (Zhao et al., 2006). However, there is no report on antiviral activity against SAR-CoV-2 of oligo-porphyran. In order to find safe and effective antiviral agent to fight COVID-19, a further purified oligo-porphyran from *P. yezoensis* was screened for its inhibitory activity against SARS-CoV-2 in the present study.

2. Materials and methods

2.1. Material

The cultured red algae *P. yezoensis* was brought from Lianyungang city, Jiangsu Province, China.

2.2. Preparation of porphyran and oligo-porphyran

Porphyran was prepared from dried algae using hot water as described previously (Zhang et al., 2003). Oligo-porphyran was degraded from porphyran using 0.5 mol/L H_2SO_4 at 80 °C for 3 h followed the method of Hou et al. (2015) with a little modification. After degradation, the solution was desalted by dialysis (MWCO = 1 kD membrane, Spectrumlabs. Inc., USA) for 48 h and then lyophilized.

2.3. The purification of oligo-porphyran

0.5 g oligo-porphyran was dissolved in water to make 10 % sugar solution, which was separated by gradient elution (0–0.3 M NaCl solution) on a DEAE-Sepharose Fast Flow column (2.6 × 60 cm) (GE, Uppsala, Sweden). The flow rate was 4.5 mL/min. A total of 387 tubes were collected by automatic partial collector with a speed of 1 min/tube. The elution curve was drawn by phenol-sulfuric acid method. According to the curve drawn, after the gradient elution of 0–0.3 M NaCl solution, three peaks were obtained, which consisted with the previous report (Hou et al., 2015).

Based on the result of gradient elution by DEAE chromatography, after calculation followed Eq. (1), oligo-porphyran was separated by DEAE-Sepharose FF column again, which was eluted with water, 0.1 M NaCl, 0.145 M NaCl and 0.2 M NaCl solution in turn. Each fraction was collected, desalted through Sepharose G-10 (Solarbio, Beijing, China) separately.

The formula for the calculation of the concentration of NaCl at peak time:

$$c = c_0\left(1 - e^{-\frac{st}{V_0}}\right) \quad (1)$$

c_0- high concentration of gradient elution; s- flow rate (mL/h); t- time (h); V_0- volume ratio of A/B vessel.

2.4. Analytical methods

Moisture content was detected by oven-drying method. Galactose (Gal) content was analyzed followed the method of Dubois, Gilles, Hamilton, Rebers, and Smith (1956). 3,6-anhydro-galactose (AnGal) content was determined according to the method of Yaphe and Arsenault (1965). Sulfated content was determined using barium chloride-gelatin method of Kawai, Seno, and Anno (1969). The molecular weight distribution was analyzed by HPLC-GPC (Shimadzu, Japan) with a TSK G3000 PWxl column (7 μm, 8.0 × 300 mm) (TOSOH, Japan) at 30 °C eluted with 0.05 M Na_2SO_4 at a flow rate of 0.5 mL/min with an RI detector. A set of Dextran Standards (2700, 5250, 9750, 13,050, 36,800 and 64,650 Da) (National Institutes for Food and Drug Control, Beijing, China) were used as the molecular weight standards. The degree of polymerization was analyzed as previously described by HPLC-HILIC on a Click-maltose column (5 μm, 4.6 × 150 mm) (Acchrom, Dalian, China) with ELSD (Geng et al., 2018).

2.5. Spectral analysis

For NMR analysis, the lyophilized sample was dissolved in D_2O (J&K Scientific Ltd., Shanghai, China) and frozen three times. ^1H and DEPT 135°-NMR were acquired on an Aglient DD2-600MHz spectrometer (Agilent, USA) at 25 °C. The relaxation delay was 2 and 1 respectively, receiver gain was 18 and 30 respectively. 2D ^1H—^1H COSY and ^1H—^{13}C HSQC were collected using the pulse program process provided by the instrument.

MALDI-TOF MS spectra was recorded with an MALDI-TOF/TOF 5800 mass spectrometer (AB Sciex, USA). The matrix used was arabinoosazone, which was successfully synthesized by our laboratory according the method reported (Chen, Baker, & Novotny, 1997). For the synthesis and verification of arabinoosazone, L-arabinose and sodium acetate were purchased from Aladdin Reagent Co., LTD (Shanghai, China), phenylhydrazine hydrochloride and DMSO-d_6 (99.9 atom % D) were purchased from Sigma-Aldrich LLC. (Darmstadt, Germany). 1 μL mixture containing 0.1 mg/mL OP145 solution in H_2O and 0.5 M arabinoosazone matrix solution in acetone was introduced on to the sample plate and air dried. Spectrum was collected in reflector negative mode, and the instrument settings was as follows: total shots, 400; accelerating voltage, 7.5 kV; laser power, 30 μJ; laser shot rate, 200 Hz. According to GPC results and several acquisitions to adjust the molecular weight set range, the final range was 800–2000.

2.6. Surface plasmon resonance (SPR) analysis

The binding affinity of OP145 with S-protein of SARS-CoV-2 was determined by SPR. A CM5 chip was placed in the chip room of the Biacore T200 instrument (GE Healthcare, Uppsala, Sweden). SARS-CoV-2 Spike S1 (D614G) recombinant protein powder (Sino Biological Inc., 40591-V02H3), lyophilized from sterile PBS, was dissolved in HBS-EP+ buffer (from 10× buffer including 0.1 M HEPES, 1.5 M NaCl, 0.03 M EDTA and 0.5 % *v*/v Surfactant P20, GE Healthcare, Uppsala, Sweden) to prepare a 400 μg/mL stock solution. The stock solution was diluted to 20 μg/mL by sodium acetate solution with pH 5.5. The chip was activated by 1-Ethyl-3-(3-dimethylaminopropyl) carbodiimide (EDC) and N-hydroxy-succinimide (NHS), and the S-protein was conjugated to channel 2 by amino coupling mode in 420 s and flow rate of 10 μL/min, and the unbound site was blocked by ethanolamine. Channel 1 was treated with the same buffer without S-protein as a blank control. OP145 was diluted from 12.5 to 6.25, 3.125, 1.56, 0.78 and 0.39 μM by PBS-P buffer (pH 7.4), and then injected at a flow rate of 30 μL/min, respectively. The contact time and dissociation time were both 60 S. The same buffer flowed over the surface of the chip to rinse unbounded sample for 60 s. The data was analyzed by Biacore T200 Evaluation Software.

2.7. Cell viability assay

The MTT [3-(4, 5-dimethylthiazol-2-yl)-2, 5-diphenyltetrazolium-bro-121mide] assay was used to determine cell viability after OP145 exposure. Briefly, HEK-293 T cells were plated onto 96-well plates with 1×10^3 cells per well. Cells were cultured in 100 μL conditioned medium and exposed to 3.91, 6.25, 12.5, 25, 100 and 400 μg/mL of OP145. After cultured for 48 h, MTT dye (10 μL, 5 mg/mL, Sigma-Aldrich, MO) was added to the culture medium. After incubation at 37 °C for 4 h, the MTT solution was removed and 100 μL DMSO was added to dissolve the formazan crystals. OD value at 490 nm was measured by Multiskan EX microplate photometer (Thermo Fisher Scientific, Waltham, MS, USA).

2.8. Pseudovirus neutralization test

The luciferase reporter assay was used to pseudovirus neutralization test followed the protocol of the pseudovirus neutralization detection kit (SC2087A, Genscript Biotechnology, Nanjing, Jiangsu, China). Firstly, positive control drug (S-protein neutralizing antibody) and OP145 were prepared to 200 μg/mL and 800 μg/mL working solution using Opti-MEM™ reduced serum medium (Opti-MEM) (Gibco Life Technologies, Grand Island, NY, USA), respectively. Then OP145 was diluted with Opti-MEM to certain concentrations (0.391, 1.563, 6.25, 25, 100 and 400 μg/mL). At the same time, positive control drug was diluted with Opti-MEM to 0.391, 1.563, 6.25, 25 and 100 μg/mL for dose-response assay according the protocol. After dilution, they were added into 96-well plate with 25 μL per well. 25 μL Opti-MEM per well was also added to the negative and blank control groups. Then pseudovirus packaged by lentivirus vector with the S-protein was diluted with Opti-MEM and was added (25 μL) into each well of positive control groups, OP145 treatment groups and negative control groups. At the same time, the same volume of Opti-MEM was added into the blank groups of the 96-well plate, followed by shaking the mixture gently, and then incubated at room temperature for 60 min. In the meanwhile, the ACE2 overexpressed target cells, Opti-HEK293/ACE2, were resuscitated and diluted to 6×10^5 cells /mL by adding DMEM complete medium containing with 10 % FBS (DMEM) (Gibco Life Technologies, Grand Island, NY, USA). The cells solution were then added to the 96-well plate with 50 μL of each well and incubated for 24 h. After 24 h, 50 μL DMEM was added to each well for another 24 h. Then, the culture medium was carefully sucked out, 50 μL luciferase chromogenic solution (combined with luciferase assay buffer and substrate from a luciferase assay kit, Promega Corporation, Madison, USA) was added quickly, and left at room temperature for 5 min. The fluorescence intensity was measured by an Infinite M1000 PRO microplate analyzer (TECAN, Switzerland). All the operation on the 96-well plate was performed in a Class II biosafety cabinet. The detail of the method process was attached to the Supplementary materials.

2.9. Molecular docking

AutoDock Vina 4.2 (Trott & Olson, 2010) was used to conduct the molecular docking between OP145 and S-protein. The X-ray crystallography structure of the S-protein from the crystal structure of SARS-CoV-2 spike receptor-binding domain (RBD) bound with ACE2 (PDB ID: 6M0J https://www.rcsb.org/structure/6M0J) was obtained as receptor. At the first step, the water molecules removement, the addition of missing paired atoms, absent hydrogens and Gasteiger charges were carried out for optimization of protein structure in the AutoDockTools-1.5.6 software. The 3D structure of the representative of tetra-sulfated octagalactose of OP145 was built and optimized by Chem3D 19.0. The ligand was docked with the prepared receptor and the absolute value of binding energy was used to represent the binding affinity. The interaction between the ligand and binding site residues was visualized by Schrodinger Maestro (Schrödinger, New York, USA).

2.10. Statistical analysis

Prism 6 (GraphPad software, USA) was used for data processing. All data were presented as the mean ± standard deviation (SD) from three independent experiments. The significance was analyzed between treatment and control groups using unpaired *t*-test. $p < 0.05$ was considered to be statistical significance.

3. Results

3.1. Preparation and analysis of oligo-porphyran

The yield of porphyran from *P. yezoensis* was 22.3 %. After degraded by dilute sulfuric acid, the yield of oligo-porphyran was 36.4 %. The GPC analysis result showed that the molecular weight of oligo-porphyran was 6.5 kD, and the sulfated content was 17 %.

The polymerization and purity of oligo-porphyran were analyzed by Click-Mal-HPLC-ELSD. Click-Mal chromatography column is a hydrophilic column with a strong specificity for the separation of carbohydrate. The chromatogram of oligo-porphyran was shown in Supporting information Fig. S1A. The separation of polymerization of oligo-porphyran was good and the degree range was large with a good reproducibility (Hou et al., 2015).

Oligo-porphyran was separated to three fractions (FF1, FF2 and FF3) after the gradient elution of 0–0.3 M NaCl solution on a DEAE-Sepharose Fast Flow column (Supporting information Fig. S1B). The HPLC analysis results (Supporting information Fig. S1C) showed that three fractions were separated fine and the polymerization degree of main compound was gradually increasing with the increase of salt concentration. In order to further purification, a specific salt concentration after calculation was used to obtain a single polymerization degree compound. The chromatogram of four fractions was shown in Fig. 1, of which the fraction eluted by 0.145 M NaCl solution (named **OP145**) performed a single peak nearly.

The GPC analysis result of OP145 showed that the single symmetrical peak with a mean weight of molecular weight (Mw) was 2.1 kD. Gal content was 68.23 %, AnGal and sulfate content was 5.20 % and 27.76 %, respectively (Table 1).

3.2. NMR analysis of OP145

NMR was confirmed to be a powerful technique for the structural analysis of porphyran. Morrice, Mclean, Long, and Williamson (1983) analyzed mono-sulfated tetrasccharide from *P. umbilicalis* using NMR first, result showed that the structure was 6-O-sulfate-α-L-Gal-(1 → 3)-β-D-Gal-(1 → 4)- 3,6-anhydro-α-L-(1 → 3)-β-D-Gal with partial methyl on C-6. The main chain structure of porphyran from different sources did not change much, only there were some differences in monosaccharide composition ratio, methylation degree and sulfate group content (Rees & Conway, 1962; Zhang et al., 2004; Zhang et al., 2005).

1D and 2D NMR analyses were employed to investigate the OP145 structure. The ^1H and ^{13}C NMR spectra are shown in Fig. 2a and b. The signals in ^1H NMR spectrum from α anomeric proton at δ 5.23 and β anomeric proton at δ 4.41 were assigned to 6- O-sulfate-α-L-Gal (L6S) and →3)-β-D-Gal (G), respectively. →3)-β-D-Gal linked to →4)-L6S was G-L6S and β-D-Gal linked to →4)-α-L-AnGal (LA) was named G-LA. There were two main signals in the anomeric region (δ 100–105), δ 103.16 and δ 100.62, which showed OP145 was mainly composed of two sugar residues. The anomeric carbon signal of β-D-galactose was observed above δ 102 ppm, while the anomeric carbon signal of α-L-galactose was observed nearby δ 100 ppm. Based on the literature data (Usov, Yarotsky, & Shashkov, 1980; Valiente, Fernandez, Perez, Marquina, & Velez, 1992), signals at δ 4.41 and δ 103.16 were assigned to H-1 and C-1 of G′, signals at δ 5.23 and δ 100.95 were assigned to H-1 and C-1 of L6S. A DEPT 135° NMR was used to investigate the presence of methylene groups (CH2), considering that the amplitude of the pulse sequence

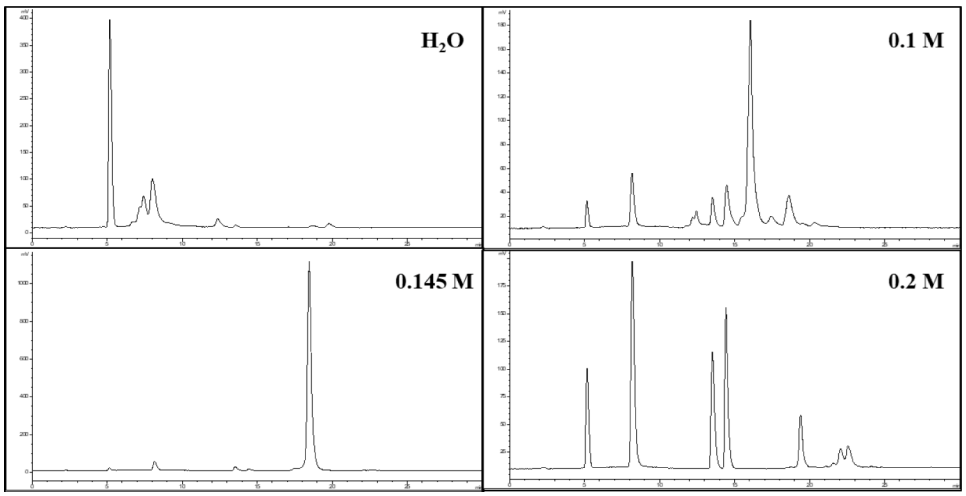

Fig. 1. The chromatogram of four fractions by Click-Mal-HPLC-ELSD obtained after separated by DEAE-Sepharose FF column, which was eluted with H_2O, 0.1 M NaCl, 0.145 M NaCl and 0.2 M NaCl solution in turn.

Table 1
The chemical composition of OP145 and porphyran.

Sample	Gal (%)	AnGal (%)	SO_4^{2-} (%)	Moisture (%)	Molecular weight[a]		
					Mw (kD)	Mn (kD)	Mw/Mn
Porphyran	74.78	21.42	8.4	10.67	133.45	655.51	4.91
OP145	68.23	5.20	27.76	5.45	2.12	1.96	1.08

[a] A set of Dextran Standards were used as the molecular weight standards, which were different to OP145 and porphyran about structure, and might cause deviation.

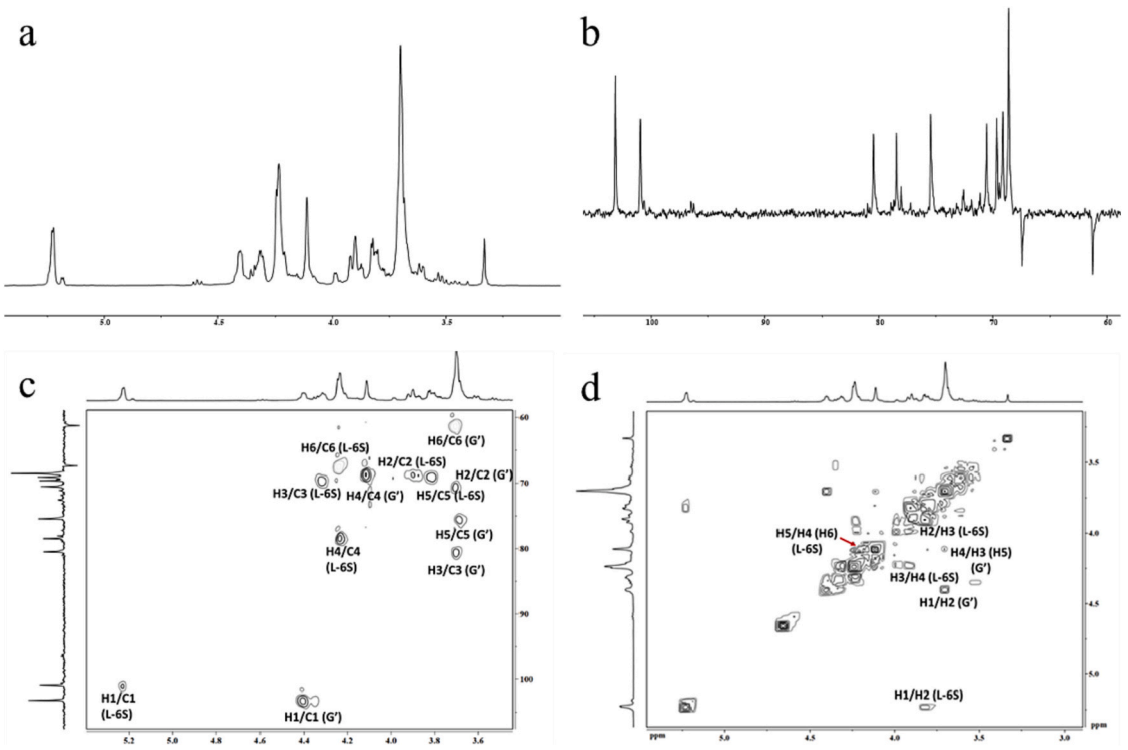

Fig. 2. The NMR spectrums of OP145 in D_2O. a) ^1H NMR, b) DEPT 135° NMR, c) HSQC and d) ^1H—^1H COSY.

signals of CH2 carbons was the opposite of CH and CH3 carbons. The DEPT 135° NMR spectrum of OP145 showed two methylene carbons signals, which were assigned as C-6 of G at δ 61.26 and C-6 of L6S at δ 67.40. No signals of O-CH_3 at δ 56–59 were observed in DEPT 135° spectrum, indicating that a significant amount of 6-*O*-methyl-galactose residue was not present in OP145. The significant migrations to the low field of chemical shifts, such as C-3 atom (δ 80.49) of G residue and C-4 atom (δ 78.47) of L6S residue, indicated the respective linkage site of

both residues, which were G-L6S. It was again confirmed that OP145 was mainly composed of two sugar residues, and the attribution of the above signal peaks was also consistent with the reports before (Barros et al., 2013; Maciel et al., 2008).

The intensity of signals somewhat reflect the content of different sugar residues. The ratio of D and L unit can be calculated on the basis of the following formula (2):

$$R_{D/L} = A_{103.16}/(A_{100.95} + A_{100.62}) \quad (2)$$

By calculating, the $R_{D/L}$ of OP145 was 1.04, which meat the molar ratio between D unit of galactose residue and L unit of galactose residue (L6S and LA) was 1: 0.96. Furthermore, the ratio of resonance strength between δ 5.23 and δ 5.18 in ^{1}H NMR spectrum was 7.7:1, which showed the molar ratio of L6S and LA. Combined the $R_{D/L}$ from DEPT 135° NMR, OP145 was composed of β-D-Gal, 6-O-sulfate-α-L-Gal and 3,6-anhydro-α-L-Gal with a molar ratio of 1:0.85:0.11. This result was consistent with the content of AnGal analyzed by chemical method.

In order to illustrate the delicate structure of OP145, the 2D NMR (^{1}H—^{13}C HSQC and ^{1}H—^{1}H COSY) were employed. The ^{1}H—^{13}C HSQC showed the correlations between C and H of G-L6S and G-LA (Fig. 2c). The correlations between H1-H6 of L6S were also observed in ^{1}H—^{1}H COSY spectrum. Furthermore, the correlation of protons of H1/H2 of G was easily detected at δ 4.41/3.69, and δ 4.11 was observed correlation with δ 3.68–3.71, which was assigned to the correlation between H3 and H4 or H5 of G linkage (Fig. 2d). The assignment of the chemical shifts was given in Table 2.

Besides, the chemical shift signals at δ 5.18 and δ 100.62 ppm in 1D NMR spectrum indicated a small amount of LA residue. However, it was difficult to identify other signals of C and H atoms because the low content and weak resonance.

3.3. MALDI-TOF MS analysis of OP145

To further clarify the structure composition of OP145, a negative-ion MALDI-TOF MS analysis was employed using arabinoosazone matrix. Although we measured the molecular weight of OP145 by HPLC-GPC, it was not appropriate when applied to MALDI-TOF MS, one of the most important reasons being that the standards and chromatographic columns used in HPLC-GPC were not very suitable for molecular weight determination of sulfate oligosaccharides. We finally choose the molecular weight range from 800 to 2000, which was best for OP145, through repeated experiments. We have summarized the corresponding compositions of the main signals and showed them in Fig. 3. MALDI-TOF MS analysis revealed OP145 contained a set of 4–10 saccharides with mostly four sulfate groups and minor three sulfate groups replacement, and with no more than two LA residues replacement. In addition, there were some high content of sulfate substitution of tri-, tetra- and pentasaccharide in OP145, which was not reported ever. Overall, OP145 is the first reported mixture of sulfated oligo-galactan, composed of sulfated tetragalactose, sulfated pentagalactose, sulfated hexagalactose, sulfated heptagalactose, sulfated octagalactose, sulfated nonagalactose and sulfated decagalactose with no more than two 3,6-anhydro-Gal replacement.

Table 2
The NMR chemical shifts affiliation of OP145.

Residues	H1/C1	H2/C2	H3/C3	H4/C4	H5/C5	H6/C6
G	4.41/ 103.16	3.69/ 70.53	3.71/ 80.49	4.11/ 68.58	3.68/ 75.45	3.69/ 61.26
L6S	5.23/ 100.95	3.83/ 69.09	3.90/ 69.63	4.23/ 78.47	4.11/ 68.58	4.23/ 67.40
LA	5.18/ 100.62	−/71.11	−/81.01	−/78.07	−/77.22	−/69.42

3.4. The binding of OP145 to S-protein of SARS-CoV-2

We use SPR analysis to detect the affinity of OP145 with S-protein. The real-time dynamic sensing diagram of OP145 binding to S-protein was shown in Fig. 4. The amount of binding with S-protein was significantly increased with the increased of OP145 concentration (0.39–12.5 μM) .And also the affinity for S-protein of OP145 increased with the extension of time to reach the saturation. The dissociation equilibrium constant (KD) was 845 nM. Association rate constant (K_a) was 3.297 × 10^4 M^{-1} S^{-1}, and dissociation rate constant (K_d) was 0.02787 S^{-1}, showed the characteristic of slow association and fast dissociation. The SPR result reflected OP145 possessed a bit strong affinity for S-protein and interacted in a dose-dependent manner.

3.5. The inhibition of OP145 against SARS-CoV-2 pseudovirus infection

SARS-CoV-2 pseudovirus neutralization assay is a rapid, flexible, reliable, sensitive, and cost-effective approach to be performed for detecting the effective neutralizing antibody, compound, peptide and drugs against SARS-CoV-2 (Donofrio et al., 2021). Thus, we used SARS-CoV-2 pseudovirus to investigate whether OP145 could neutralize the S-protein of SARS-CoV-2 to prevent the binding of S-protein to ACE2 receptor of the target cell *in vitro*. The S-protein of the SARS-CoV-2 was lentivirus-packaged on the surface of pseudovirus, so the pseudovirus could bind to ACE2 overexpressed reconstructive target cells (Opti-HEK293/ACE2 cells) to simulate the novel coronavirus cell-cell and cell-cell membrane fusion process. After infecting the target cells, the pseudovirus can express the luciferase gene carried in the target cell, and the number of cells infected by the pseudovirus can be inferred by detecting the chemical signal of the reaction between luciferase and the substrate. When the candidate drug binds to S-protein, the target cells infected by pseudovirus and the signal of luciferase decreases, thus the ability of the sample to neutralize SARS-CoV-2 virus can be concluded.

Under this premise, the effect of OP145 on the inhibition of the binding of S-protein to ACE2 was shown in Fig. 5. When the concentration was above 1.563 μg/mL, OP145 could significantly reduce the luciferase signal intensity with EC50 of 37.52 μg/mL (Fig. 5a), which corresponds to ~17.8 nM, indicating that OP145 could competitively inhibit the binding of S-protein to ACE2, and then inhibit the entry of SARS-CoV-2 virus into cells. The S-protein neutralizing antibody, which could bind to the RBD of S-protein and further inhibit the infection of pseudovirus to Opti-HEK293/ACE2 cells, was used as positive control. As shown in Fig. 5b, positive control inhibited the binding of S-protein to ACE2 effectively. At the same time, OP145 showed an inhibitory activity to a certain extent, and such inhibition was not owed to the toxicity to HEK293 cells (Fig. 5c).

3.6. Molecular docking

According the structure analysis result, OP145 was a mixture of a serial oligo-galactan, so we conducted the primary tetra-sulfated octa-galactose (Gal_8S_4) to do the docking experiment. The result of molecular docking simulation was shown in Fig. 6a. The RBD's amino acid residues of S-protein involved in binding the ACE2 could bind to OP145 and showed a binding energy of −5.1 kcal.mol^{-1}. Interaction analysis revealed that OP145 had six hydrogen bonds interacting with Arg403, Gly496, Gln498, Tyr505 and Asp405 (Table 3, Fig. 6b). The molecular docking result also confirmed the slightly tight binding between OP145 and S-protein which consistent with the binding assay *in vitro*.

4. Discussion

After extraction, degradation and purification, a more homogeneous oligo-porphyran with a mean molecular weight of 2.1 kD, named OP145, was separated from *P. yezoensis*. The chemical analysis result showed that OP145 was mainly composed of Gal and sulfate groups with

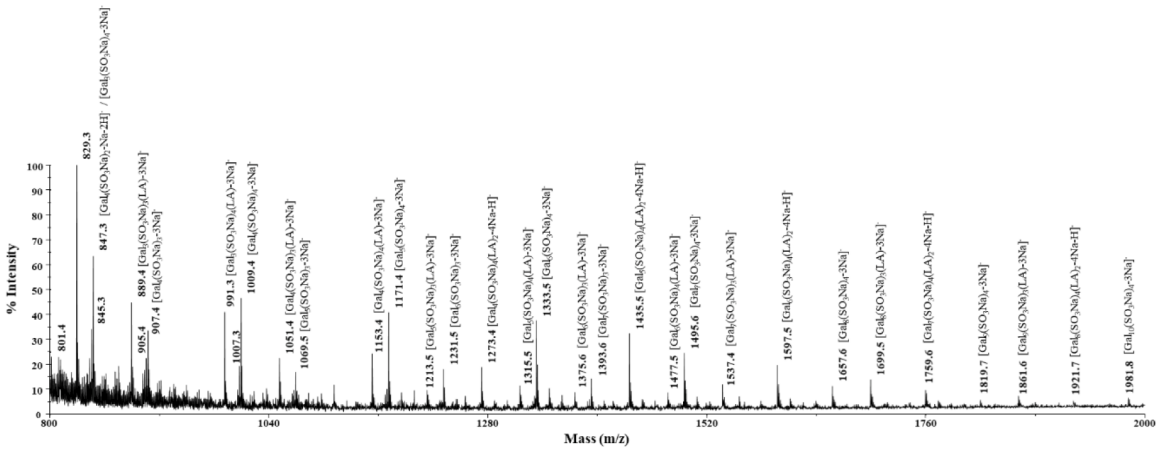

Fig. 3. Negative-ion MALDI-TOF MS of OP145 (arabinoosazone matrix).

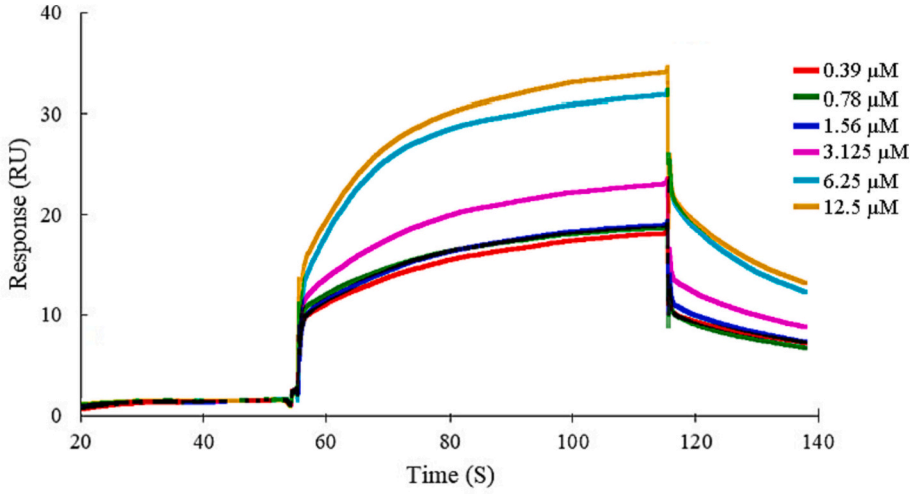

Fig. 4. Surface plasmon resonance sensorgram showing the binding affinity for OP145 and S-protein. Data are shown by the best fit of a 1:1 binding model.

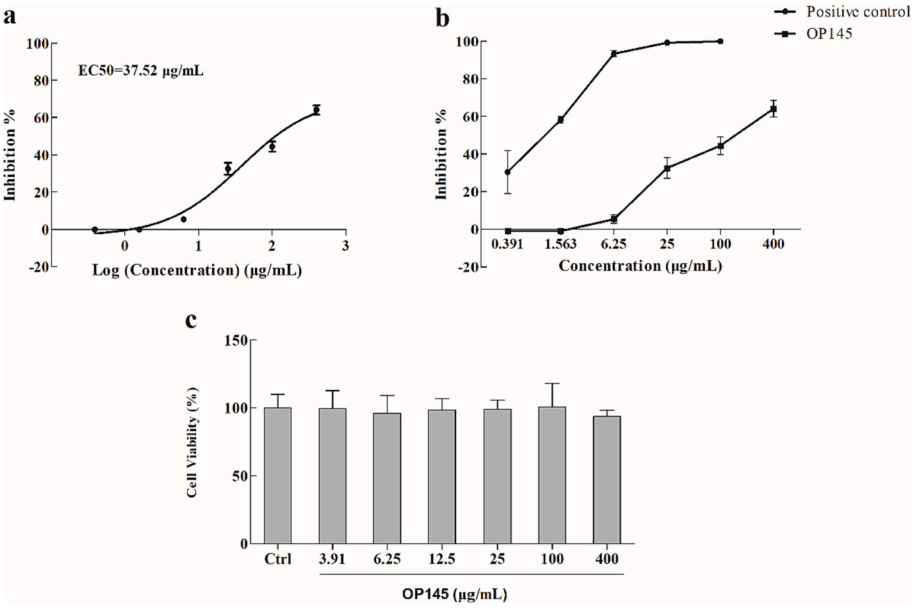

Fig. 5. Inhibitory activity of OP145 against the binding of SARS-CoV-2 pseudovirus S-protein to ACE2 target cells. **a)** The EC50 curve of the inhibition of viral infection by OP145. **b)** The inhibition of positive control and OP145 at the diluted concentrations. The inhibition percentage was calculated following the formula: Inhibition (%) = $[1-(L_{positive/OP145}-L_{blank})/(L_{negative}-L_{blank})] \times 100$ %, L means the luminescence intensity. **c)** The cell viability of OP145 on HEK-293T cells at different concentrations. Standard deviations were based on triplicate experiments.

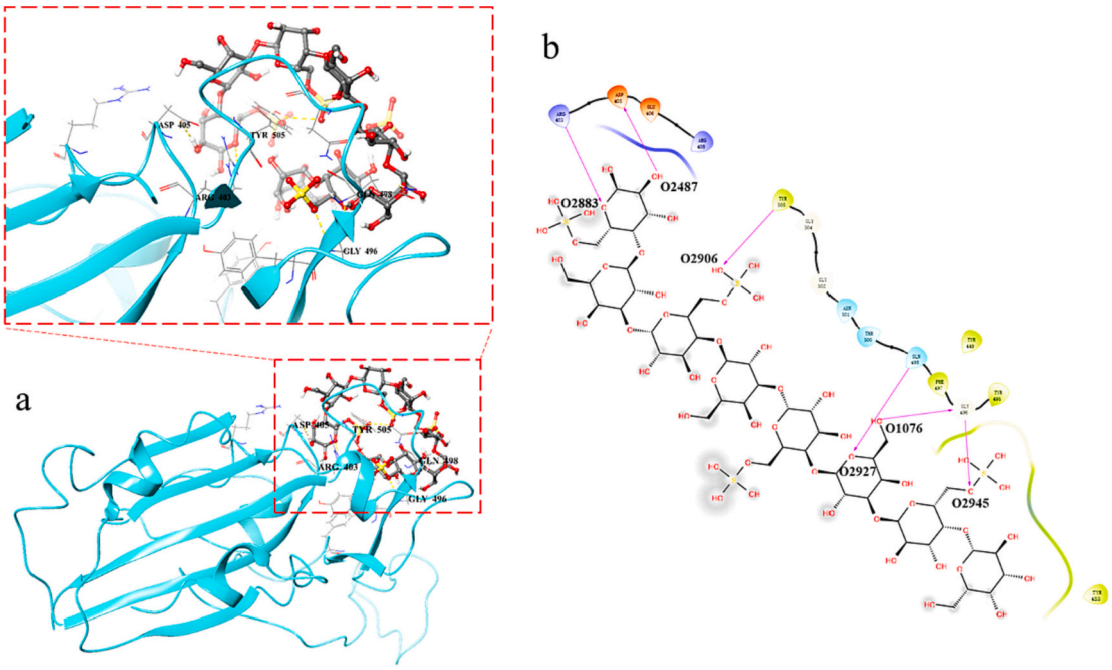

Fig. 6. Molecular docking simulation of OP145 and RBD of S-protein represented as chain and the magnified view of the RBD shows the possible interacting residues in <5 Å vicinity with OP145 (a). The hydrogen bonds (purple) formed between OP145 and the interacting residues of S-protein (b).

Table 3
Hydrogen bonds formed between OP145 and S-protein.

Donor atom	Acceptor atom	Distance (Å)
S: Arg403: HH22	O: O2883	1.82
S: Gly496: H	O: O2945	2.30
S: Gln498: HE21	O: O2927	2.70
S: Tyr505: HH	O: O2906	2.43
O: O2487	S: Asp405: OD2	2.14
O: O1076	S: Gly496: O	1.94

68.23 % and 27.76 %, and a minor of LA (5.20 %). 1D and 2D NMR showed the notably serial chemical shifts of G′ and L6S, and OP145 was composed of G, L6S and LA with a molar ratio of 1: 0.85: 0.11 according the calculation of peaks density. MALDI-TOF MS analysis revealed the component of OP145, a mixture of mainly a series tetrasulfate-oligogalactan and minor trisulfate-oligogalactan including tri-, tetra-, penta-, hexa-, hepta-, octa-, nona- and deca-galactose with partially no more than two LA replacement. Combined with the results, we first isolated the high sulfate-substituted oligo-porphyran from *P. yezoensis*.

Recently, marine sulfated oligosaccharides are considered to be able to compensate for the poor solubility and unclear structure of MSP and have attracted more and more attention (Zhu, Ni, Xiong, & Yao, 2020). Most importantly, low toxicity and low-cost marine glycans and oligo-glycans have demonstrated potent antiviral activities through multiple molecular mechanisms (Hao et al., 2019). Salih et al. (2021) subjected ten sulfated glycans to molecular docking and dynamic simulation experiments, and ascertained their potential interactions with the RBD of SARS CoV-2, including sulfated galactan. In fact, the molecular structure of those five sulfated glycans were simplified, replaced by corresponding tetra-oligosaccharide in the report, because it was impossible to draw an accurate structure of such marine derived glycans. Here, we obtained the specific oligo-galactose from *P. yezoensis*, indeed, OP145 possessed good solubility and clearer structure.

The inhibitory activity of OP145 against SARS-CoV-2 was investigated *in vitro*. SPR technique could reflect the interaction between the purpose receptor and samples with un-labeling (Rusnati & Presta, 2015). The SPR result showed that the KD of OP145 to S-protein of SARS-CoV-2 was 845 nM with a dose-dependent manner, which meant a bit slight binding activity. We speculated that the binding of OP145 to S-protein could somewhat prevent the binding of S-protein to ACE2 to reduce infection. The pseudovirus test result confirmed the competitively inhibitory activity of OP145 on the binding of S-protein to ACE2 with EC50 of 37.52 μg/mL, which corresponds to ~17.8 nM, and OP145 could inhibit the entry of SARS-CoV-2 virus into cells further. Antiviral activities correlated with the SPR results. Ge et al. (2021) identified that doxepin at the concentration of 20 μM could inhibit SARS-CoV-2 spike pseudovirus from entering the ACE2-expressing cell, reducing the infection rate to 25.82 % through the pseudovirus assay.

Molecular docking simulation could predict the conformational binding energy of ligands to receptor using matching and scoring algorithms *in silico* and occupies a prominent role in early drug discovery process (Leach, Shoichet, & Peishoff, 2006). Tetra-sulfated octagalactose, a main component of OP145, was illustrated to do the molecular docking experiment. Our study revealed that OP145 bound to S-protein RBD of SARS-CoV-2 with a binding energy of −5.1 kcal.mol^{-1}, and interacted with Arg403, Gly496, Gln498, Tyr505 and Asp405 by hydrogen bonds through the oxygen atoms of hemiacetal, C-2 oxhydryl, C-6 oxhydryl and sulfate group. All the results indicated that OP145 was found to be an inhibitor of SARS-CoV-2 and has good development potential.

However, the activity need to be further improved. The chain length of oligosaccharide and polysaccharide was an important factor in the anti-virus and immunological property. Such situation was also reported about fucoidan (Kwon et al., 2020), that the smaller RPI-28, which had the same basic structure as RPI-27 but a lower molecular weight, possessed lower antiviral activity against SARS-CoV-2 with EC50 = 1.2 μM, while the EC50 of RPI-27 was ~83 nM. Wang, Feng, An, Gu, and Guo (2015) also reported the synthesized free oligosaccharides were proven to be low immunogenic compared to the corresponding polysaccharide constituted the bacteria cell wall, but after conjugation with a carrier protein, the oligosaccharides showed the immunological properties.

5. Conclusion

In the present study, a more homogeneous oligosaccharide was isolated and purified from *Pyropia yezoensis* with a mean Mw of 2.1 kD. Chemical analysis, 1 D and 2D NMR, MALDI-TOF MS techniques revealed that OP145 was mainly composed of β-D-Gal, α-L-Gal (6S) and 3,6-anhydro-α-L-Gal with the molar ratio of 1:0.85:0.11. Furthermore, OP145 was a mixture of series of major tetrasulfate-oligogalactan and minor trisulfate-oligogalactan (Dp = 4–10) with no more than two 3,6-anhydro-α-L-Gal replacement. *In vitro* and *in silico* experiments indicated that OP145 possessed inhibitory activity against SARS-CoV-2, and could bind to S-protein to prevent the binding between S-protein and ACE2. Although OP145 did not show very competitive activity, the safety and solubility make further structural confirmation and optimization of OP145, as well as further activity testing *in vitro* and *in vivo*, very important to fully explore OP145 as structurally based oligosaccharides against SARS-CoV-2.

CRediT authorship contribution statement

Lihua Geng: Investigation, resources, data curation, formal analysis, writing. **Quanbin Zhang**: Project administration, writing - review & editing. **Qishan Suo**: Investigation, data analysis. **Jing Wang**: Funding acquisition, supervision, validation. **Yingxia Wang**: Methodology, MALDI-TOF analysis. **Cong Wang**: Methodology, NMR analysis. **Ning Wu**: Investigation, project administration, funding acquisition, Writing - original draft.

Declaration of competing interest

The authors declare that they have no known competing financial interests or personal relationships that could have appeared to influence the work reported in this paper.

Data availability

I have shared the link to my data at the Attached File step.

Acknowledgments

This research was supported by the National Key Research and Development program of China (Grant number 2019YFD0900705), Shandong Provincial Natural Science Foundation (No. ZR2019BD053), Science and Technology program of Nantong (MS12021037) and Special Open Fund of Laboratory for Marine Biology and Biotechnology, Qingdao Pilot National Laboratory for Marine Science and Technology (No. OF2020NO02).

Appendix A. Supplementary data

Supplementary data to this article can be found online at https://doi.org/10.1016/j.carbpol.2022.120173.

References

Bansal, S., Jonsson, C. B., Taylor, S. L., Figueroa, J. M., Dugour, A. V., Palacios, C., & César Vega, J. (2020). *Iota-carrageenan and Xylitol inhibit SARS-CoV-2 in cell culture*. https://doi.org/10.1101/2020.08.19.225854. BioRxiv, 2020.08.19.225854.

Barros, F. C. N., Da Silva, D. C., Sombra, V. G., MacIel, J. S., Feitosa, J. P. A., Freitas, A. L. P., & De Paula, R. C. M. (2013). Structural characterization of polysaccharide obtained from red seaweed *Gracilaria caudata* (J Agardh). *Carbohydrate Polymers, 92*, 598–603. https://doi.org/10.1016/j.carbpol.2012.09.009

Bouhlal, R., Haslin, C., Chermann, J. C., Colliec-Jouault, S., Sinquin, C., Simon, G., … Bourgougnon, N. (2011). Antiviral activities of sulfated polysaccharides isolated from *Sphaerococcus coronopifolius* (Rhodophytha, Gigartinales) and *Boergeseniella thuyoides* (Rhodophyta, Ceramiales). *Marine Drugs, 9*(7), 1187–1209. https://doi.org/10.3390/md9071187

Chen, P., Baker, A. G., & Novotny, M. V. (1997). The use of osazones as matrices for the matrix-assisted laser desorption/ionization mass spectrometry of carbohydrates. *Analytical Biochemistry, 244*(1), 144–151. https://doi.org/10.1006/abio.1996.9874

Donofrio, G., Franceschi, V., Macchi, F., Russo, L., Rocci, A., Marchica, V., Costa, F., Giuliani, N., Ferrari, C., & Missale, G. (2021). A simplified SARS-CoV-2 pseudovirus neutralization assay. *Vaccines, 9*, 389. https://doi.org/10.3390/vaccines9040389

Dubois, M., Gilles, K. A., Hamilton, J. K., Rebers, P. A., & Smith, F. (1956). Colorimetric method for determination of sugars and related substances. *Analytical Chemistry, 28*(3), 350–356. https://doi.org/10.1021/ac60111a017

Ge, S., Wang, X., Hou, Y., Lv, Y., Wang, C., & He, H. (2021). Repositioning of histamine H1 receptor antagonist: Doxepin inhibits viropexis of SARS-CoV-2 spike pseudovirus by blocking ACE2. *European Journal of Pharmacology, 896*(76), Article 173897. https://doi.org/10.1016/j.ejphar.2021.173897

Geng, L., Wang, J., Zhang, Z., Yue, Y., & Zhang, Q. (2019). Structure and bioactivities of porphyrans and oligoporphyrans. *Current Pharmaceutical Design, 25*(11), 1163–1171. https://doi.org/10.2174/1381612825666190430111725

Geng, L., Zhang, Q., Wang, J., Jin, W., Zhao, T., & Hu, W. (2018). Glucofucogalactan, a heterogeneous low-sulfated polysaccharide from *Saccharina japonica* and its bioactivity. *International Journal of Biological Macromolecules, 113*, 90–97. https://doi.org/10.1016/j.ijbiomac.2018.02.008

Hao, C., Yu, G., He, Y., Xu, C., Zhang, L., & Wang, W. (2019). Marine glycan–based antiviral agents in clinical or preclinical trials. *Reviews in Medical Virology, 29*, Article e2043. https://doi.org/10.1002/rmv.2043

Hou, Y., Wang, J., Simerly, T., Jin, W., Zhang, H., & Zhang, Q. (2015). Hydrogen peroxide released from *Pyropia yezoensis* induced by oligo-porphyrans: Mechanisms and effect. *Journal of Applied Phycology, 27*(4), 1639–1649. https://doi.org/10.1007/s10811-014-0471-7

Kawai, Y., Seno, N., & Anno, K. (1969). A modified method for chondrosulfatase assay. *Analytical Biochemistry, 32*(2), 314–321. https://doi.org/10.1016/0003-2697(69)90091-8

Kwon, P. S., Oh, H., Kwon, S. J., Jin, W., Zhang, F., Fraser, K., Hong, J. J., Linhardt, R. J., & Dordick, J. S. (2020). Sulfated polysaccharides effectively inhibit SARS-CoV-2 in vitro. *Cell Discovery, 6*(1), 4–7. https://doi.org/10.1038/s41421-020-00192-8

Leach, A. R., Shoichet, B. K., & Peishoff, C. E. (2006). Prediction of protein-ligand interactions. Docking and scoring: Successes and gaps. *Journal of Medicinal Chemistry, 49*(20), 5851–5855. https://doi.org/10.1021/jm060999m

Liu, Y., Geng, L., Zhang, J., Wang, J., Zhang, Q., Duan, D., & Zhang, Q. (2018). Oligo-porphyran ameliorates neurobehavioral deficits in parkinsonian mice by regulating the PI3K/Akt/Bcl-2 pathway. *Marine Drugs, 16*(3), 1–16. https://doi.org/10.3390/md16030082

Maciel, J. S., Chaves, L. S., Souza, B. W. S., Teixeira, D. I. A., Freitas, A. L. P., Feitosa, J. P. A., & de Paula, R. C. M. (2008). Structural characterization of cold extracted fraction of soluble sulfated polysaccharide from red seaweed *Gracilaria birdiae*. *Carbohydrate Polymers, 71*(4), 559–565. https://doi.org/10.1016/j.carbpol.2007.06.026

Mazumder, S., Ghosal, P. K., Pujol, C. A., Carlucci, M. J., Damonte, E. B., & Ray, B. (2002). Isolation, chemical investigation and antiviral activity of polysaccharides from *Gracilaria corticata* (Gracilariaceae, Rhodophyta). *International Journal of Biological Macromolecules, 31*(1–3), 87–95. https://doi.org/10.1016/S0141-8130(02)00070-3

Morokutti-Kurz, M., Fröba, M., Graf, P., Große, M., Grassauer, A., Auth, J., Schubert, U., & Prieschl-Grassauer, E. (2021). Iota-carrageenan neutralizes SARS-CoV-2 and inhibits viral replication in vitro. *PLoS ONE, 16*(2), Article e0237480. https://doi.org/10.1371/journal.pone.0237480

Morrice, L. M., Mclean, M. W., Long, W. F., & Williamson, F. B. (1983). Porphyran primary structure: An investigation using β-agarase I from *Pseudomonas atlantica* and ^{13}C-NMR spectroscopy. *European Journal of Biochemistry, 133*(3), 673–684. https://doi.org/10.1111/j.1432-1033.1983.tb07516.x

Qiu, Y., Jiang, H., Fu, L., Ci, F., & Mao, X. (2021). Porphyran and oligo-porphyran originating from red algae *Porphyra*: Preparation, biological activities, and potential applications. *Food Chemistry, 349*, Article 129209. https://doi.org/10.1016/j.foodchem.2021.129209

Rees, D. A., & Conway, E. (1962). The structure and biosynthesis of porphyran: A comparison of some samples. *The Biochemical Journal, 84*(1), 411–416. https://doi.org/10.1042/bj0840411

Rusnati, M., & Presta, M. (2015). Angiogenic growth factors interactome and drug discovery: The contribution of surface plasmon resonance. *Cytokine and Growth Factor Reviews, 26*(3), 293–310. https://doi.org/10.1016/j.cytogfr.2014.11.007

Salih, A. E. M., Thissera, B., Yaseen, M., Hassane, A. S. I., El-seedi, H. R., Sayed, A. M., & Rateb, M. E. (2021). Marine sulfated polysaccharides as promising antiviral agents: A comprehensive report and modeling study focusing on SARS CoV-2. *Marine Drugs, 19*(8). https://doi.org/10.3390/md19080406

Singh, R., Chauhan, N., & Kuddus, M. (2021). Exploring the therapeutic potential of marine-derived bioactive compounds against COVID-19. *Environmental Science and Pollution Research, 28*, 52798–52809.

Song, S., Peng, H., Wang, Q., Liu, Z., Dong, X., Wen, C., Ai, C., Zhang, Y., Wang, Z., & Zhu, B. (2020). Inhibitory activities of marine sulfated polysaccharides against SARS-CoV-2. *Food and Function, 11*(9), 7415–7420. https://doi.org/10.1039/d0fo02017f

Trott, O., & Olson, A. J. (2010). AutoDock Vina: Improving the speed and accuracy of docking with a new scoring function, efficient optimization, and multithreading. *Journal of Computational Chemistry, 31*(2), 455–461. https://doi.org/10.1002/jcc.21334

Usov, A. I., Yarotsky, S. V., & Shashkov, A. S. (1980). ^{13}C-NMR spectroscopy of red algal galactans. *Biopolymers, 19*, 977–990.

Valiente, O., Fernandez, L. E., Perez, R. M., Marquina, G., & Velez, H. (1992). Agar polysaccharides from the red seaweeds *Gracilaria domingensis* Sonder ex Kützing and *Gracilaria mammillaris* (Montagne) Howe. *Botanica Marina, 35*(2), 77–82. https://doi.org/10.1515/botm.1992.35.2.77

Wang, J., Hou, Y., Duan, D., & Zhang, Q. (2017). The structure and nephroprotective activity of oligo-porphyran on glycerol-induced acute renal failure in rats. *Marine Drugs, 15*(5), 135. https://doi.org/10.3390/md15050135

Wang, L., Feng, S., An, L., Gu, G., & Guo, Z. (2015). Synthetic and immunological studies of mycobacterial lipoarabinomannan oligosaccharides and their protein conjugates. *Journal of Organic Chemistry, 80*(20), 10060–10075. https://doi.org/10.1021/acs.joc.5b01686

Wang, S., Wang, W., Hou, L., Qin, L., He, M., Li, W., & Mao, W. (2020). A sulfated glucuronorhamnan from the green seaweed *Monostroma nitidum*: Characteristics of its structure and antiviral activity. *Carbohydrate Polymers, 227*, Article 115280. https://doi.org/10.1016/j.carbpol.2019.115280

Wang, X., Liu, D., Wang, Z., Cai, C., Jiang, H., & Yu, G. (2021). Porphyran-derived oligosaccharides alleviate NAFLD and related cecal microbiota dysbiosis in mice. *FASEB Journal, 35*(6), Article e21458. https://doi.org/10.1096/fj.202000763RRR

Witvrouw, M., Este, J. A., Mateu, M. Q., Reymen, D., Andrei, G., Snoeck, R., … De Clercq, E. (1994). Activity of a sulfated polysaccharide extracted from the red seaweed *Aghardhiella tenera* against human immunodeficiency virus and other enveloped viruses. *Antiviral Chemistry and Chemotherapy, 5*(5), 297–303. https://doi.org/10.1177/095632029400500503

World Health Organization. (2020). *Coronavirus disease (COVID-19) situation reports*. WHO. https://covid19.who.int/.

Yaphe, W., & Arsenault, G. P. (1965). Improved resorcinol reagent for the determination of fructose, and of 3,6-anhydrogalactose in polysaccharides. *Analytical Biochemistry, 13*, 143–148. https://doi.org/10.1016/0003-2697(65)90128-4

Zhang, Q., Qi, H., Zhao, T., Deslandes, E., Ismaeli, N. M., Molloy, F., & Critchley, A. T. (2005). Chemical characteristics of a polysaccharide from *Porphyra capensis* (Rhodophyta). *Carbohydrate Research, 340*(15), 2447–2450. https://doi.org/10.1016/j.carres.2005.08.009

Zhang, Q. B., Li, N., Liu, X. G., Zhao, Z. Q., Li, Z., & Xu, Z. H. (2004). The structure of a sulfated galactan from *Porphyra haitanensis* and its in vivo antioxidant activity. *Carbohydrate Research, 339*(1), 105–111. https://doi.org/10.1016/j.carres.2003.09.015

Zhang, Q. B., Yu, P. Z., Li, Z., Zhang, H., Xu, Z. H., & Li, P. C. (2003). Antioxidant activities of sulfated polysaccharide fractions from *Porphyra haitanesis*. *Journal of Applied Phycology, 15*(4), 305–310. https://doi.org/10.1023/a:1025137728525

Zhao, T. T., Zhang, Q. B., Qi, H. M., Zhang, H., Niu, X. Z., Xu, Z. H., & Li, Z. (2006). Degradation of porphyran from *Porphyra haitanensis* and the antioxidant activities of the degraded porphyrans with different molecular weight. *International Journal of Biological Macromolecules, 38*(1), 45–50. https://doi.org/10.1016/j.ijbiomac.2005.12.018

Zhu, B., Ni, F., Xiong, Q., & Yao, Z. (2020). Marine oligosaccharides originated from seaweeds: Source, preparation, structure, physiological activity and applications. *Critical Reviews in Food Science and Nutrition, 61*(1), 60–74. https://doi.org/10.1080/10408398.2020.1716207